LETTER

doi:10.1038/nature09402

Decay of aftershock density with distance does not indicate triggering by dynamic stress

Keith Richards-Dinger[1], Ross S. Stein[2] & Shinji Toda[3]

Resolving whether static[1–3] or dynamic[4–8] stress triggers most aftershocks and subsequent mainshocks is essential to understand earthquake interaction and to forecast seismic hazard[9]. Felzer and Brodsky[10] examined the distance distribution of earthquakes occurring in the first five minutes after $2 \le M < 3$ and $3 \le M < 4$ mainshocks and found that their magnitude $M \ge 2$ aftershocks showed a uniform power-law decay with slope −1.35 out to 50 km from the mainshocks. From this they argued that the distance decay could be explained only by dynamic triggering. Here we propose an alternative explanation for the decay, and subject their hypothesis to a series of tests, none of which it passes. At distances more than 300 m from the $2 \le M < 3$ mainshocks, the seismicity decay 5 min before the mainshocks is indistinguishable from the decay five minutes afterwards, indicating that the mainshocks have no effect at distances outside their static triggering range. Omori temporal decay, the fundamental signature of aftershocks, is absent at distances exceeding 10 km from the mainshocks. Finally, the distance decay is found among aftershocks that occur before the arrival of the seismic wave front from the mainshock, which violates causality. We argue that Felzer and Brodsky[10] implicitly assume that the first of two independent aftershocks along a fault rupture triggers the second, and that the first of two shocks in a creep- or intrusion-driven swarm triggers the second, when this need not be the case.

Aftershocks can be distinguished from other earthquakes only by Omori decay with time following the mainshock, and by a density that decays roughly with distance from the mainshock rupture. The spatial correlation of calculated Coulomb stress change with aftershocks off the rupture surface[2,11–13], and the temporal correlation with tidal stresses, which lack a dynamic component[14], provide evidence that increased static stress promotes aftershocks. The occurrence of earthquakes during the passage of the surface waves, at distances up to 35 rupture lengths from their mainshocks and thus well beyond the static range, provides evidence for dynamic earthquake triggering[4,6,8,15,16]. Nevertheless, remotely triggered aftershocks and tremor have been detected in California[6] and Japan[17] only when large mainshocks excite low-frequency (>15 s) energy; if correct, this would preclude $M < 3$ earthquakes as sources of remote dynamic triggering, particularly at distances of up to 350 rupture lengths from the mainshocks (50 km/150 m), as claimed by Felzer and Brodsky[10].

Felzer and Brodsky[10] argued that the observed seismicity density with distance (Fig. 1a) is a product of the decay of seismic wave amplitude, which in southern California has a power-law slope of about −1.2 (ref. 18). Unlike typical plots with a single mainshock and many aftershocks, in Fig. 1a only one in 70 mainshocks has a single aftershock, and so these aftershocks are, if nothing else, rare. Felzer and Brodsky[10] select as a mainshock any event that is not preceded by a larger shock within 3 days and 100 km, and not followed by a larger shock within 12 h and 100 km, although these windows are changed in some of their analyses. An aftershock is any $M \ge 2$ earthquake that is smaller than and occurs within 5 min (or 30 min) of a $2 \le M < 4$ mainshock. They plot the linear density of the identified aftershocks as a function of distance. This process, and their linear density calculation, is explained in Supplementary Fig. 1. Because we will argue that most pairs of selected earthquakes do not each comprise a mainshock and its aftershock, we will refer to events identified by the Felzer and Brodsky[10] criteria as 'mainshocks' and 'aftershocks' to differentiate them from events for which the identification is unambiguous.

Because the static stress decays to nearly zero within a kilometre of the $M < 3$ mainshocks (red curve, Fig. 1a), the principal argument of Felzer and Brodsky[10] is that the observed power-law distance decay can be caused only by dynamic triggering of aftershocks far from the mainshock rupture. But two independent (that is, primary) aftershocks on a fault rupture that coincidentally occur far apart but within a short time of each other, shown schematically in Fig. 1c, qualify as a 'mainshock–aftershock' pair (a primary aftershock and its secondary) by the Felzer and Brodsky[10] criteria, even though the first did not trigger the second. In Fig. 1b and in the online-only Methods we show that a combination of observed Gutenberg–Richter *b*-values, constant stress-drop magnitude to rupture-area scaling[19], and aftershock productivity that scales with mainshock magnitude[20], also give power-law distance distributions out to 50 km, even when aftershocks are

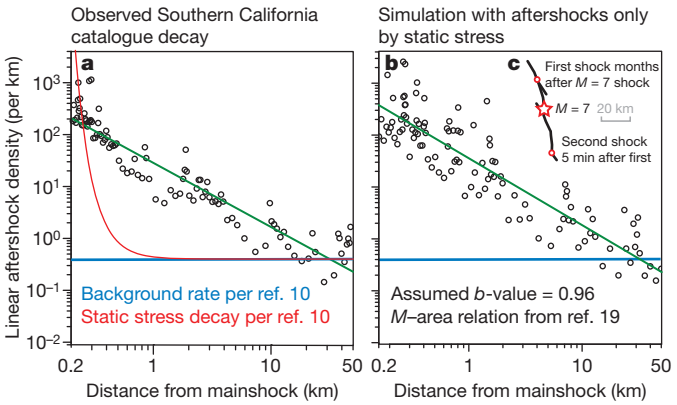

Figure 1 | Alternative explanations for the distance decay of seismicity density. **a**, Seismicity decay using the distance ranges of Felzer and Brodsky[10], from which it was argued that the aftershocks must be dynamically triggered. Data is from the Southern California catalogue: 7,134 $2 \le M < 3$ mainshocks, 101 $M \ge 2$ aftershocks, 0–5 min period. The blue line in both panels is the background rate according to ref. 10. The green line in both panels shows the power-law decay over 0.2–50 km: **a**, −1.24; **b**, −1.29. **b**, Simulation with aftershocks caused by static stress. The same decay as in **a** can arise without any remote dynamic or even off-fault triggering; here, aftershocks are distributed uniformly on mainshock rupture surfaces, with the number of aftershocks produced by a mainshock of M proportional to $10^{0.8M}$. The M–area relationship is from ref. 19. The Gutenberg–Richter *b*-value is set to 0.96, as observed for the Southern California catalogue. **c**, Did the first shock trigger the second, as assumed in **a**, or were both primary aftershocks of the $M = 7$ event that happened to strike 5 min apart? When applied over many mainshocks, the latter circumstance results in the decay shown in **b**.

[1]Department of Earth Sciences, University of California, Riverside, California 92521, USA. [2]US Geological Survey, Menlo Park, California 94025, USA. [3]Disaster Prevention Research Institute, Kyoto University, Gokasho, Uji, Kyoto 611-0011, Japan.

restricted to the fault rupture surfaces and so explicitly exclude remote dynamic triggering. Reasonable values of these parameters lead to power-law decay exponents of −1 to −2, encompassing those observed in California (Fig. 1a) and Japan (Fig. 2a). So, to discriminate between these alternatives we conduct a series of tests, using the Felzer and Brodsky[10] selection criteria unless otherwise noted (Supplementary Table 1 gives the catalogue parameters).

The 5 min before the mainshocks includes all possible earthquake and aseismic interactions except those caused by the mainshock itself, and so if the 5-min period after the mainshocks captures aftershocks as claimed by Felzer and Brodsky[10], then the 5 min before the mainshocks should not exhibit the same density and slope (Fig. 3a and b). But at distances greater than 300 m, the Southern California decay curves before and after the 'mainshocks' are indistinguishable (Fig. 3c). The 300 m distance corresponds to one to two source dimensions for $2 \leq M < 3$ mainshocks[21], which means that the mainshocks have no discernible effect on subsequent seismicity except within the distance of static triggering. The 'mainshocks' in Fig. 3a might be regarded by Felzer and Brodsky[10] as aftershocks that happen to be larger than their mainshocks (that is, the triggered shock is larger than the triggering shock), and so could display the same decay slope. But because aftershocks are only rarely larger than their mainshocks, the decay curve should be shifted downward in Fig. 3a relative to that in Fig. 3b, which is not observed. The time series of shocks outside the static range (Supplementary Fig. 2) also shows that the seismicity rate before and after the mainshocks is constant at distances more than 1 km from the mainshocks, as would be expected if there were no remote aftershock triggering.

If the distant earthquakes are indeed aftershocks of their mainshocks, they should undergo Omori temporal decay[22] as do virtually all aftershock sequences, including the remotely triggered aftershocks of the 1992 Landers earthquake that occurred in the Long Valley caldera,

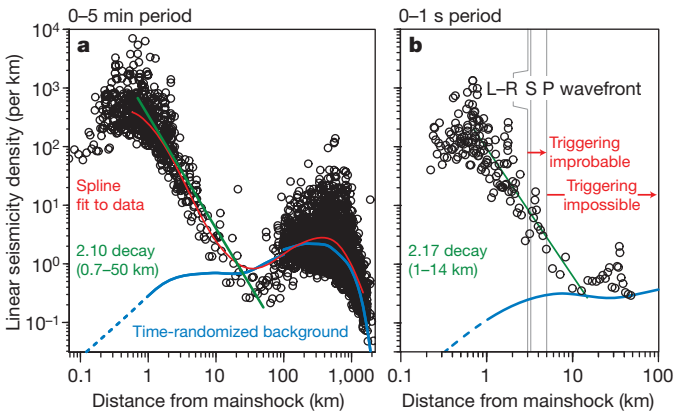

Figure 2 | Distance decay in Japan during 5-min and 1-s periods. **a**, Unlike Felzer and Brodsky[10], we use only JMA events with timing errors <0.1 s, which reduces location uncertainty to 275 m, and we adopt the appropriate 0.7 completeness magnitude[27,28] (Supplementary Fig. 4). Data is from the JMA catalogue: 7,839 $0.7 \leq M < 3$ mainshocks and 2,494 $M \geq 0.7$ aftershocks, 0–5 min period. To estimate the background (blue line), we randomly select 5-min intervals from the JMA catalogue and associate these with the 'mainshocks' selected using the Felzer and Brodsky[10] criteria rather than using the 5 min after each 'mainshock.' The green line in both panels shows the power-law decay: **a**, −2.10 (over 0.7–50 km); **b**, −2.17 (over 1–14 km). The red line in **a** shows the spline fit to the data. **b**, The same decay is seen before aftershocks can be triggered. Data is from the JMA catalogue: 193,603 $M < 5$ mainshocks, 171 $M < 5$ aftershocks, 0–1 s time period. Because earthquakes lost through inadequate detection are not important for this test, we use all $M < 5$ events to maximize the number of aftershocks, use aftershocks smaller or larger than their mainshocks, and use 1-h exclusion times before and after mainshocks. The 1-h window is nevertheless 3,600 times longer than the 1-s period, more stringent than the factor of 864 (3 days/5 min) used by Felzer and Brodsky[10]. L–R is the Love–Rayleigh wave.

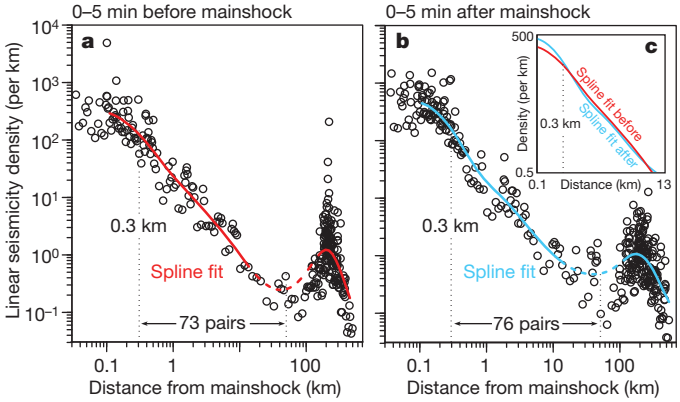

Figure 3 | Comparison of earthquakes 5 min before and after mainshocks. Data is from the Southern California catalogue: 7,134 $2 \leq M < 3$ 'mainshocks', 319 $M \geq 2$ 'foreshocks' in **a**, 364 $M \geq 2$ 'aftershocks' in **b**, 0–5 min period, over full distance range. To ensure that no data are common to both plots, we exclude first and second shocks of the same magnitude. The decays over 0.2–50 km are 1.32 ± 0.09 (**a**) and 1.24 ± 0.09 (**b**); where dashed, the spline fit is uncertain. **c**, The splines in **a** and **b** are indistinguishable except at distances less than 300 m from the mainshocks, and there are about the same number of pairs over 300 m–50 km.

400 km away[23]. Aftershocks within the static range (<1 km of their mainshocks) display Omori decay (Fig. 4a), but Japan Meteorological Agency (JMA) catalogue 'aftershocks' located 10–50 km from their mainshocks do not (Fig. 4b). For southern California, once the year of seismicity after the two $M > 7$ shocks is removed (comprising 10% of the 'mainshocks' and 21% of the 'mainshock–aftershock' pairs), Omori decay all but disappears (Supplementary Fig. 3). The inland JMA catalogue lacks any $M \geq 7$ mainshocks. The first year of the $M \geq 7$ sequences provides the largest number of independent primary aftershocks that can be mistaken for 'mainshock–aftershock' pairs (Fig. 1c). If the Omori decay were indeed associated with aftershocks of $M \leq 3$ mainshocks, then excluding the first year after $M \geq 7$ shocks would have no impact.

Earthquakes that occur before the wave train from the mainshock arrives cannot be aftershocks, and so should not exhibit the same decay if it is caused by triggering. Most earthquakes unambiguously triggered by teleseismic waves begin seconds after the surface (Love–Rayleigh) wave arrival; shear (S)-wave triggering is rare and compressional (P)-wave triggering is all but unknown[6,8,16]. Yet the power-law distance

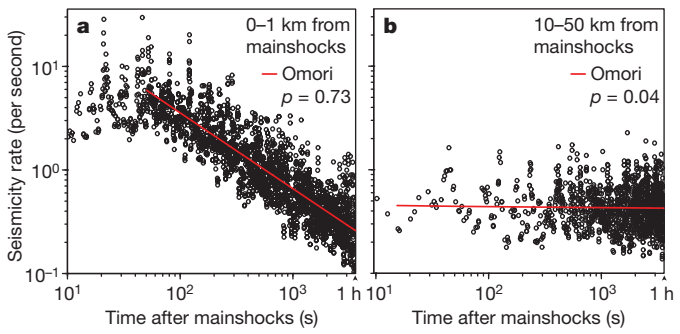

Figure 4 | Omori decay for near-field and remote seismicity. Each plotted point represents a 5-point moving average (lag = 5). The red line in both panels shows the calculated Omori decay exponent. **a**, Omori temporal decay becomes clear beginning about 40 s after the mainshocks. Decays asymptote to the independently determined background rate. **b**, Even during the first 5 min, remote 'aftershocks' do not exhibit Omori decay. For 4–50 km, the Omori $p = 0.22$. All observations are shown. There is also no Omori decay for $1.5 \leq M < 3.0$. For southern California, see Supplementary Fig. 3. Data is from the JMA catalogue for the time period 0–5 min: **a**, 2,325 shocks 0–1 km from $0.7 \leq M < 3$ mainshocks; **b**, 1,404 shocks 10–50 km from $0.7 \leq M < 3$ mainshocks.

decay is seen before the arrival of the surface waves at seismicity densities well above the expected background rates, and there is no discontinuity of the decay across the wavefront boundary (Fig. 2b). The decay curve extends to the calculated background at 13 km, even though the P-wave reaches only 5 km. Three-quarters of the JMA 'aftershocks' that occur before the Love wave arrival lie in rupture zones of earlier large mainshocks or at swarm sites (Supplementary Fig. 4), suggesting that many of the nominal 'mainshock–aftershock' pairs are instead independent primary aftershocks of excluded mainshocks (Fig. 1c), and swarm events triggered by creep or intrusions[24–26] (Fig. 5a).

Consistent with the JMA observations, the highest rate of southern California 'aftershocks' located more than 10 km from their 'mainshocks' occurs within 0–6 s of the 'mainshocks', even though the Rayleigh wave does not even reach 10 km until 3.3 s after the 'mainshock' (Supplementary Fig. 2). A disproportionate number of the Southern California 'mainshock–aftershock' pairs lie in rupture zones of larger preceding mainshocks or in swarm sites (Fig. 5b), a further indication of the misattribution of a triggering relationship. Some 56% of the pairs have at least one shock in an aftershock zone of an excluded mainshock or in an independently identified swarm zone, even though only 32% of the 'mainshocks' locate in these zones. Similarly, a disproportionate number of the pairs occur during the year after large mainshocks or during swarms (Fig. 5b and Supplementary Fig. 5).

For each of these tests, the observations are consistent with the alternative hypothesis of coincident and static-triggered aftershocks shown in Fig. 1b and c: for two coincident independent aftershocks or two swarm events triggered by a non-seismic process, in which the first did not trigger the second event, the 5 min before the first event would be identical to the 5 min afterwards. There would be a higher rate of aftershocks only within the range of static stress, which for $M < 3$ mainshocks is <300 m. Second, there should be no Omori decay from the time of the first shock, because the subsequent events are not its aftershocks. Finally, the second event of any coincident pair could occur before the arrival of waves from the first, because the second was not triggered by the first.

Taken together, we believe these tests (as well as others furnished in Supplementary Figs 6–8) falsify the hypothesis that only dynamic triggering can explain the power-law decay of aftershocks of $2 \leq M < 4$ mainshocks to 50 km during the ensuing 5 or 30 min. We suggest instead that the distance decay is primarily a selection artefact that assumes that primary, independent aftershocks of larger mainshocks have triggered each other. We emphasize that we are not suggesting that dynamic triggering does not occur, but only that the observed distance decay provides no evidence for it.

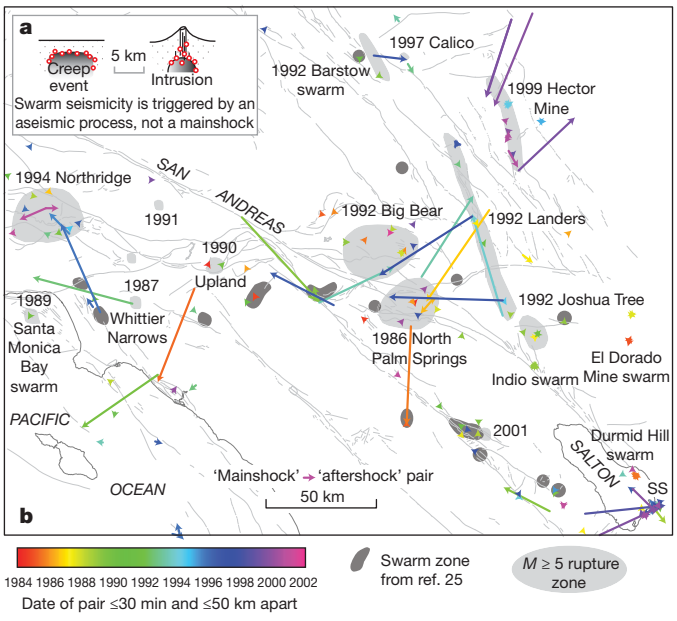

Figure 5 | Map of nominal 'mainshock–aftershock' pairs. a, The Felzer and Brodsky[10] selection criteria do not remove swarms when they are not triggered by a mainshock[24–26]. **b**, Southern California pairs in the region where the majority occurs; most pairs locate in the rupture zones of large shocks or in swarm sites. Because vectors are projected onto a map, the horizontal vectors give minimum distances. One might ask why there are not more long vectors in the $M \geq 7$ aftershock zones, but in a power-law distribution, shorter arrows dominate. One could also ask why there are long vectors connecting isolated shocks. But for vectors of 40 km, the background rate is equal to the nominally triggered rate (Fig. 1a), so half of these vectors should be random background. SS, the Salton Sea swarm site.

METHODS SUMMARY

We reproduce the algorithms of Felzer and Brodsky[10] to select 'mainshocks' and 'aftershocks' by their criteria, and to calculate the linear seismicity density; both procedures are explained graphically in Supplementary Fig. 1. We can almost exactly replicate their results for southern California and Japan if we use their catalogue parameters (Supplementary Table 1 gives their parameters and ours). But because events identified by the Felzer and Brodsky[10] selection criteria as 'mainshock–aftershock' pairs could instead be independent (for example, primary) aftershocks of larger excluded mainshocks with no triggering relationship to each other, we also derive the expected distribution of distances if all aftershocks were restricted to the mainshock rupture surface, and thus no remote dynamic triggering occurred at all. In the online-only Methods section, we derive an expression for the distribution of mainshock rupture lengths assuming a Gutenberg–Richter distribution of magnitudes, Wells–Coppersmith[19] magnitude-to-rupture length scaling (which for small earthquakes is equivalent to constant stress-drop scaling), and aftershock productivity that scales with mainshock magnitude[20]. We then plot the resulting decay of linear seismicity density for aftershocks produced by each mainshock that survive Felzer and Brodsky[10] selection, assuming either a line source, or rectangular planes as in the realization of Fig. 1b. In Supplementary Figs 6–8, we also test assertions by Felzer and Brodsky[10] that 2 days of aftershocks of $5 < M \leq 6$ mainshocks exhibit a power-law decay to 500 km, and that 30 min of aftershocks of $M < 5$ shocks and 30 days of aftershocks following $M > 6$ mainshocks cannot be explained by static rate/state Coulomb stress triggering.

Full Methods and any associated references are available in the online version of the paper at www.nature.com/nature.

Received 16 June; accepted 4 August 2010.

1. Stein, R. S. The role of stress transfer in earthquake occurrence. *Nature* **402,** 605–609 (1999).
2. Toda, S., Stein, R. S., Richards-Dinger, K. & Bozkurt, S. Forecasting the evolution of seismicity in southern California: animations built on earthquake stress transfer. *J. Geophys. Res.* **110,** B05S16, doi: 10.1029/2004JB003415 (2005).
3. Parsons, T. Global observation of Omori-law decay in the rate of triggered earthquakes: large aftershocks outside the classical aftershock zone. *J. Geophys. Res.* **107,** doi: 10.1029/2001JB000646 (2002).
4. Hill, D. P. *et al.* Seismicity remotely triggered by the magnitude 7.3 Landers, California, earthquake. *Science* **260,** 1617–1623 (1993).
5. Kilb, D. A strong correlation between induced peak dynamic coulomb stress change from the 1992 M7.3 Landers, California, earthquake and the hypocenter of the 1999 M7.1 Hector Mine, California earthquake. *J. Geophys. Res.* **108,** 10.1029/2001JB000678 (2003).
6. Brodsky, E. E. & Prejean, S. G. New constraints on mechanisms of remotely triggered seismicity at long valley caldera. *J. Geophys. Res.* **110,** B04302, doi: 04310.01029/02004JB003211 (2005).
7. Gomberg, J. & Johnson, P. Dynamic triggering of earthquakes. *Nature* **437,** 830 (2005).
8. Hill, D. P. & Prejean, S. G. in *Treatise on Geophsyics* (ed. Kanamori, H.) Vol. 4, 257–291 (Elsevier, 2007).
9. Freed, A. M. Earthquake triggering by static, dynamic, and postseismic stress transfer. *Annu. Rev. Earth Planet. Sci.* **33,** 335–367 (2005).
10. Felzer, K. R. & Brodsky, E. E. Decay of aftershock density with distance indicates triggering by dynamic stress. *Nature* **441,** 735–738 (2006).
11. Hardebeck, J. L., Nazareth, J. J. & Hauksson, E. The static stress change triggering model: constraints from two southern California aftershocks sequences. *J. Geophys. Res.* **103,** 24427–24437 (1998).
12. Ma, K.-F., Chan, C.-H. & Stein, R. S. Response of seismicity to coulomb stress triggers and shadows of the 1999 Mw=7.6 Chi-Chi, Taiwan, earthquake. *J. Geophys. Res.* **110,** doi: 10.1029/2004JB003389 (2005).
13. Helmstetter, A., Kagan, Y. Y. & Jackson, D. D. Importance of small earthquakes for stress transfers and earthquake triggering. *J. Geophys. Res.* **110,** B05S08, doi: 10.1029/2004JB003286 (2005).

14. Cochran, E. S., Vidale, J. E. & Tanaka, S. Earth tides can trigger shallow thrust fault earthquakes. *Science* **306,** 1164–1166 (2004).
15. Brodsky, E., Karakostas, V. & Kanamori, H. A new observation of dynamically triggered regional seismicity: Earthquakes in Greece following the August, 1999 Izmit, Turkey earthquake. *Geophys. Res. Lett.* **27,** 2741–2744 (2000).
16. Velasco, A. A., Hernandez, S., Parsons, T. & Pankow, K. Global ubiquity of dynamic earthquake triggering. *Nature Geosci.* **1,** 375–379, doi: 10.1038/ngeo204 (2008).
17. Miyazawa, M. & Brodsky, E. E. Deep low-frequency tremor that correlates with passing surface waves. *J. Geophys. Res.* **113,** B01307, doi: 01310.01029/02006JB004890 (2008).
18. Jennings, P. C. & Kanamori, H. Effect of distance on local magnitudes found from strong-motion records. *Bull. Seismol. Soc. Am.* **73,** 265–280 (1983).
19. Wells, D. L. & Coppersmith, K. J. New empirical relationships among magnitude, rupture length, rupture width, rupture area, and surface displacement. *Bull. Seismol. Soc. Am.* **84,** 974–1002 (1994).
20. Felzer, K. R., Abercrombie, R. E. & Ekström, G. Secondary aftershocks and their importance for aftershock forecasting. *Bull. Seismol. Soc. Am.* **93,** 1433–1448 (2003).
21. Abercrombie, R. E. Earthquake source scaling relationships from -1 to 5 m_l using seismograms recorded at 2.5-km depth. *J. Geophys. Res.* **100,** 24015–24036 (1995).
22. Marsan, D. & Lengliné, O. Extending earthquakes' reach through cascading. *Science* **319,** 1076–1079 (2008).
23. Hill, D. P., Johnston, M. J. S., Langbein, J. O. & Bilham, R. Response of Long Valley caldera to the Mw = 7.3 Landers, California, earthquake. *J. Geophys. Res.* **100,** 12985–13005 (1995).
24. Toda, S., Stein, R. S. & Sagiya, T. Evidence from the A.D. 2000 Izu Islands swarm that seismicity is governed by stressing rate. *Nature* **419,** 58–61 (2002).
25. Vidale, J. E. & Shearer, P. M. A survey of 71 earthquake bursts across southern California: exploring the role of pore fluid pressure fluctuations and aseismic slip as drivers. *J. Geophys. Res.* **111,** B05312, doi: 05310.01029/02005JB004034 (2006).
26. Lohman, R. B. & McGuire, J. J. Earthquake swarms driven by aseismic creep in the Salton trough, California. *J. Geophys. Res.* **112,** B04405, doi: 04410.01029/02006JB004596 (2007).
27. Woessner, J. & Wiemer, S. Assessing the quality of earthquake catalogues: estimating the magnitude of completeness and its uncertainty. *Bull. Seismol. Soc. Am.* **95,** 684–698 (2005).
28. Wiemer, S. & Wyss, M. Minimum magnitude of completeness in earthquake catalogs: examples from Alaska, the western United States, and Japan. *Bull. Seismol. Soc. Am.* **90,** 859–869 (2000).

Supplementary Information is linked to the online version of the paper at www.nature.com/nature.

Acknowledgements We thank K. Felzer, E. Brodsky, D. Jackson, S. Steacy, J. Hardebeck, R. Harris, and I. Main for comprehensive reviews; and Z. Peng, J. Vidale and Y. Okada for comments.

Author Contributions The authors contributed equally to the manuscript.

Author Information Reprints and permissions information is available at www.nature.com/reprints. The authors declare no competing financial interests. Readers are welcome to comment on the online version of this article at www.nature.com/nature. Correspondence and requests for materials should be addressed to K.R.-D. (keithrd@ucr.edu).

METHODS

Expected aftershock distance-decay in the absence of remote dynamic triggering. Because the events identified by the selection criteria of Felzer and Brodsky[10] as mainshock–aftershock pairs could plausibly instead be temporally coincident independent (primary) aftershocks of some previous mainshock, we here derive the expected distribution of distances between pairs of such events. We show that standard and reasonable choices of the relevant parameters lead to distributions which are power laws with a range of exponents that encompasses those seen in the earthquake data.

We denote the distance between two such events (that is, two independent aftershocks of a previous mainshock) as l and their probability distribution function (PDF) by $\phi_l(l)$. Note that ϕ_l, being a PDF, is normalized to integrate to 1, but that it is a linear density and differs from the linear seismicity density calculated from the data only in the normalization. To derive this distribution we will need both the distribution of distances between aftershocks of a mainshock of a given size, and the distribution of those mainshock sizes. In this derivation we will mostly work in a two-dimensional setting and so we use rupture length, L, as the measure of mainshock size, but the results are similar in three dimensions, in which one can represent mainshocks as squares or rectangles (as we show in Fig. 1b).

To derive an expression for the distribution of mainshock rupture lengths, $\phi_L(L)$, we will begin with the typical Gutenberg–Richter distribution of magnitudes:

$$\phi_M(M) = b\ ln(10) \times 10^{-b(M-M_c)} \text{ for } M \geq M_c \quad (1)$$

where b is the Gutenberg–Richter b-value and M_c is the magnitude of completeness. This is the distribution of magnitudes of all events, but what we need is the distribution of magnitudes of the earlier events that give rise to pairs of nearly coincident aftershocks that are misidentified by the Felzer and Brodsky[10] selection criteria as 'mainshock–aftershock' pairs; we will denote this distribution by $\phi'_M(M)$. This distribution will be different from that of all events for at least two reasons: first, larger events produce more aftershocks, and second, the fraction of aftershocks produced by a mainshock that survive the Felzer and Brodsky[10] selection criteria and therefore are misidentified as mainshock–aftershock pairs may vary with mainshock magnitude. Denoting the relative number of aftershocks produced by a mainshock of magnitude M by $p(M)$ and the fraction of aftershocks of a magnitude M mainshock that survive the selection criteria by $f(M)$, we have

$$\phi'_M(M) \propto \phi_M(M)p(M)f(M) \quad (2)$$

The number of aftershocks produced by a mainshock of magnitude M, $p(M)$, is often found (or taken) to be proportional to $10^{\alpha M}$, with $\alpha \approx 1$ (refs 13, 29 and 30). The form of $f(M)$ is harder to predict, though it would seem likely to be a decreasing function of M (that is, larger mainshocks probably have a larger fraction of their aftershocks eliminated by the selection criteria because of their more productive aftershock sequences). Because $\phi_M(M)$ and $p(M)$ are both exponential, we will here assume that $f(M)$ is also exponential, so that the effect of multiplying by $f(M)$ is to modify the exponent. Specifically, in what follows we will take the product $p(M)f(M)$ to be proportional to $10^{\alpha' M}$, and most probably $0 \leq \alpha' \leq \alpha$. This gives:

$$\phi'_M(M) = (b-\alpha')\ ln(10) \times 10^{(-b+\alpha')(M-M_c)} \text{ for } M \geq M_c \quad (3)$$

The next step is to derive the distribution of rupture lengths $\phi_L(L)$ of those events that produce pairs of aftershocks that survive the Felzer and Brodsky[10] selection criteria. Given a relation between rupture length and magnitude $M = M(L)$, ϕ_L will be given by the fundamental transformation law of probability densities[31]:

$$\phi_L(L) = \phi'_M(M(L)) \cdot \left|\frac{dM}{dL}\right| \quad (4)$$

If we assume a standard empirical relation between rupture length and magnitude[19], which is roughly equivalent to uniform stress-drop scaling:

$$M = 4.38 + 1.49 \log_{10}(L) \quad (5)$$

then we have:

$$\phi_L(L) = \frac{1.49(b-\alpha')}{L_c}\left(\frac{L}{L_c}\right)^{1.49(-b+\alpha')-1} \text{ for } L \geq L_c \quad (6)$$

with the obvious definition of L_c such that $M_c = 4.39 + 1.48 \log_{10}(L_c)$, (that is, L_c is the rupture length of an event with magnitude M_c).

To obtain $\phi_l(l)$, the distribution of the distances l between these coincident aftershocks, we need to know $\phi_{l|L}(l,L)$ (that is, the conditional distribution of l for a given L). For a specific $\phi_{l|L}(l,L)$ we obtain $\phi_l(l)$ via a standard rule relating marginal distributions to conditional distributions[31]:

$$\phi_l(l) = \int_{-\infty}^{\infty} \phi_{l|L}(l,L)\phi_L(L)dL \quad (7)$$

Next, we explore what sorts of $\phi_l(l)$ result from choosing $\phi_{l|L}(l,L)$ that are consistent with static stress triggering by an event with rupture length L. As an illustrative oversimplification, if aftershocks were uniformly distributed along the rupture surface (that is, a line of length L), with no off-fault aftershocks at all, then the distribution of the distance between two randomly chosen aftershocks would be given by:

$$\phi_{l|L}(l,L) = \frac{2}{L}\left(1-\frac{l}{L}\right) \text{ for } 0 \leq l \leq L \quad (8)$$

This arises because the PDF of the difference of two independent random variables is the cross-correlation of the individual PDFs, and, in this case, the individual PDFs of the event locations are rectangles that are non-zero between 0 and L. Thus, the PDF of the difference of the two locations is a triangle centred on the origin (that is, non-zero between $-L$ and L). However, the distance between them is the absolute value of this difference, resulting in a triangle which is non-zero only between 0 and L. This form of $\phi_{l|L}(l,L)$ results in a $\phi_l(l)$ given by:

$$\begin{aligned}\phi_l(l) &= \int_{-\infty}^{\infty} \phi_{l|L}(l,L)\phi_L(L)dL \\ &= \int_{\max(l,L_c)}^{\infty} \frac{2}{L}\left(1-\frac{l}{L}\right)\frac{1.49(b-\alpha')}{L_c}\left(\frac{L}{L_c}\right)^{-1.49(b-\alpha')-1} dL \\ &= \begin{cases} \frac{2 \cdot 1.49(b-\alpha')}{L_c}\left(\frac{1}{1.49(b-\alpha')+1} - \frac{1}{1.49(b-\alpha')+2}\left(\frac{l}{L_c}\right)\right) & \text{for } 0 \leq l \leq L_c \\ \frac{2 \cdot 1.49(b-\alpha')}{L_c}\left(\frac{1}{1.49(b-\alpha')+1} - \frac{1}{1.49(b-\alpha')+2}\right)\left(\frac{l}{L_c}\right)^{-1.49(b-\alpha')-1} & \text{for } l \geq L_c \end{cases}\end{aligned} \quad (9)$$

Note that this is a power law with a slope of $1.49(-b+\alpha')-1$ for $l \geq L_c$. For reasonable bounds on α' and for $b \approx 1$, this slope will range from approximately -1 (for $\alpha' = 1$), to approximately -2.5 (for $\alpha' = 0$), encompassing the range of power-law slopes observed in the Southern California (Fig. 1a) and Japanese (Fig. 2a) catalogue data.

We show two realizations of ϕ_l in Supplementary Fig. 1; in Supplementary Fig. 1f we distribute aftershocks uniformly along a line to compare it with the analytic derivation above, and, perhaps more realistically, in Supplementary Fig. 1g we uniformly distribute aftershocks on rectangular rupture areas. For both realizations we draw event magnitudes from a Gutenberg–Richter distribution with a b-value of 0.96, the mean value we calculate for the Southern California catalogue. We then use $\alpha' = 0.65$ to choose the number of aftershocks produced by each event that survive the selection criteria. In Supplementary Fig. 1f, each mainshock is assigned a length L from equation (5), and the aftershocks are uniformly distributed along a line of this length. In Supplementary Fig. 1g, each mainshock is assigned an area from the relation[19] $A = 10^{(M-4.07)/0.98}$ km^2 and assigned a square rupture area up to a size of 15 km × 15 km and a rectangular area (with a width of 15 km) for larger areas. The aftershocks are then uniformly distributed over the rupture area. Note in Supplementary Fig. 1f, for which we have an analytic prediction, the prediction is in good agreement with the sampled empirical distribution. Most important, the slopes of the lines fitted to the linear part of the distributions are in the range seen for actual earthquake data. Note also that in real data the behaviour at small separations will be strongly affected by location errors.

Tests of arguments advanced in the Supplementary Information of ref. [10]. We find a distance-decay slope of -2.10 for the JMA catalogue (Fig. 2a), whereas Felzer and Brodsky[10] report a slope of -1.45 in their Supplementary Fig. 6a. Our steeper slope arises because Felzer and Brodsky[10] did not make any cutoff for location or timing errors, and as a result their catalogue includes offshore earthquakes with poor locations and depths. This leads to noisy measurements of 'mainshock–aftershock' distance when the events are within a few kilometres of each other, distorting the decay slope. By our reckoning, their mean three-dimensional location error is 1,760 m (they report "2.2 km at 98% confidence", and so these estimates are in rough agreement). In contrast, we used earthquakes with timing errors <0.1 s, which removed all offshore and outer island events; our resulting mean location error is 908 m. We examined the JMA catalogue to benefit from its larger area, higher earthquake rates, and denser station coverage; this coverage permits a lower completeness magnitude, which we calculate[27,28] to be 0.7 (shown in Supplementary Fig. 4a), whereas Felzer and Brodsky[10] consider $M > 2.5$ 'aftershocks.' But the minimum magnitude is not the reason that we find a steeper slope than they do; when we use $M > 2.5$, we find a slope of -2.16 ± 0.30, indistinguishable from that for $M > 0.7$. Because the Southern California catalogue has order-of-magnitude

smaller location errors, no such cutoffs are needed and our distance decay slope agrees with that of Felzer and Brodsky[10].

In Supplementary Fig. 6, we test the argument of Felzer and Brodsky[10] (their Supplementary Fig. 5) that 2 days of $M \geq 3$ aftershocks of $5 < M \leq 6$ mainshocks exhibit a power-law decay to 500 km. The nine "$M = 5$–6" mainshocks in their compilation are not identified, and there are only 6 'aftershocks' beyond 10 km. We instead analyse aftershocks of the 28 September 2004 $M = 6.1$ Parkfield earthquake, which are complete to $M = 1.1$ starting 15 min after the mainshock[32], and so provide ten times the data used in their figure; there is also no ambiguity about choosing the fault plane from the nodal planes or the extent of the mainshock rupture. The Parkfield aftershock distance-decay merges with the background at 20–30 km from the edges of the rupture surface in Supplementary Fig. 6, and is well fitted by a static rate/state Coulomb stress model; there is no indication of a decay extending hundreds of kilometres from the rupture.

Felzer and Brodsky[10] analyse the period of 30 min–25 days following $3 \leq M < 4$ mainshocks in their Supplementary Fig. 4d to argue that over this longer time period, the distance-decay remains consistent with a -1.4 power-law decay, but with a larger contribution from background earthquakes. They fit the data with a curve $\rho(r) = cr^{-1.4} + b$, where b is the background rate and r is distance; their plots extend to 12 km. In fact, the data do not asymptote to zero beyond 12 km as implied by this equation, but instead peak at the mean radius of the seismic network because the background is not flat in linear density, as we show with the blue curves in Fig. 2a (Japan) and Fig. 3 (southern California). But the 25-day period they selected enables us to consider $M \geq 1.2$ earthquakes following six southern California $6.0 \leq M \leq 7.3$ earthquakes with finite fault rupture models[2] and with aftershocks complete within several days of their mainshocks, which we show in our Supplementary Fig. 7. The Landers and Hector Mine earthquakes alone contribute 15,000 aftershocks, 200 times more than in the plots of Felzer and Brodsky[10]. These $M \geq 6$ aftershock decays are well fitted by static rate/state Coulomb stress, and none show uniform power-law decays except very roughly over the range of 2–30 km. The correlation coefficients between observation and the static stress model are high, and the regression slope is close to 1.

In their Supplementary Fig. 3, Felzer and Brodsky[10] argue that the power law distance decay extends to at least 16 km from $2 \leq M < 3$ and $3 \leq M < 4$ 'mainshocks' for 30 min. Regardless of whether they are triggered by static or dynamic stress, the maximum distance of triggered aftershocks should increase with mainshock magnitude. Using their 30-min period, we find a magnitude dependence on aftershock distance in our Supplementary Fig. 8, but only out to about 1 km from the mainshock hypocentres for mainshocks. These observations are well fitted by static stress-drop source scaling[21], which simply means that most aftershocks occur within or near the periphery of the mainshock rupture. The absence of the dependence beyond 1 km is, in our judgment, incompatible with remote dynamic triggering to 16 km.

29. Helmstetter, A. & Sornette, D. Subcritical and supercritical regimes in epidemic models of earthquake aftershocks. *J. Geophys. Res.* **107,** 2237, doi: 10.1029/2001JB001580 (2002).
30. Felzer, K., Abercrombie, R. & Ekström, G. Secondary aftershocks and their importance for aftershock forecasting. *Bull. Seismol. Soc. Am.* **93,** 1433–1448 (2003).
31. Kendall, M. & Stuart, A. *The Advanced Theory of Statistics* Vol. 1 *Distribution Theory* Ch. 1 (Hafner, 1969).
32. Peng, Z. & Zhao, P. Migration of early aftershocks following the 2004 parkfield earthquake. *Nature Geosci.* **2,** doi: 10.1038/ngeo1697 (2009).